This article has been accepted for publication in IEEE Robotics and Automation Letters. This is the author's version which has not been fully edited and content may change prior to final publication. Citation information: DOI 10.1109/LRA.2023.3270036

Hybrid Force-Impedance Control for Fast End-Effector Motions

Maged Iskandar, Christian Ott, Alin Albu-Schäffer, Bruno Siciliano, and Alexander Dietrich

***Abstract*—Controlling the contact force on various surfaces is essential in many robotic applications such as in service tasks or industrial use cases. Mostly, classical impedance and hybrid motion-force control approaches are employed for these kinds of physical interaction scenarios. In this work, an extended Cartesian impedance control algorithm is developed, which includes geometrical constraints and enables explicit force tracking in a hybrid manner. The unified framework features compliant behavior in the free (motion) task directions and explicit force tracking in the constrained directions. Advantageously, the involved force subspace in contact direction is fully dynamically decoupled from dynamics in the motion subspace. The experimental validation with a torque-controlled robotic manipulator on both flat and curved surfaces demonstrates the performance during highly dynamic desired trajectories and confirms the theoretical claims of the approach.**

***Index Terms*—Force control, Hybrid motion force control, High-speed robot polishing, Contact control, Robot force control.**

I. Introduction

Well-defined physical interaction with the environment is an essential requirement for a vast number of real-world applications in robotics. Interaction control can be performed directly to realize desired time-dependent or constant contact forces or indirectly by specifying a dynamic behavior of the controlled robot during physical interaction, e. g., through impedance [1] or admittance control [2]. Hence, interaction forces indirectly result from active control of the physical parameters of the robot, i. e., inertia, damping, and stiffness.

Generally, the approach of impedance control [1] has been extensively employed in interaction scenarios with various extensions that have been developed over the last decades. The concept allows for active compliance to cope with environmental uncertainty and can provide passive interaction. In classical impedance control, one can deliberately exert desired forces and torques on the environment by either shifting the desired position (virtual position) or adding a feed-forward force on top of the nominal control action. This means that the external forces are not necessarily considered in the controller design in an explicit way. Multiple techniques aim for set-point generation and modulation to achieve indirect force control [3], [4] or to enhance human comfort during physical interaction [5], [6]. In combination with indirect force control, differential geometry-based methods can be exploited to realize contact impedance on arbitrarily curved surfaces [7].

Manuscript received: December 21, 2022; revised March 21, 2023; accepted April 13, 2023.

This paper was recommended for publication by Editor Jaydev Desai upon evaluation of the Associate Editor and Reviewers' comments. This work is partially supported by the ERC through euROBIN under Grant 101070596 and partially supported by MOTIE/KEIT under Numbers 20014485 and 20014398.

M. Iskandar, C. Ott, A. Albu-Schäffer, and A. Dietrich are with the German Aerospace Center (DLR), (maged.iskandar@dlr.de), B. Siciliano is with University of Naples Federico II, Italy, A. Albu-Schäffer is also with TU Munich, and C. Ott is also with TU Wien.

Digital Object Identifier (DOI): see top of this page.

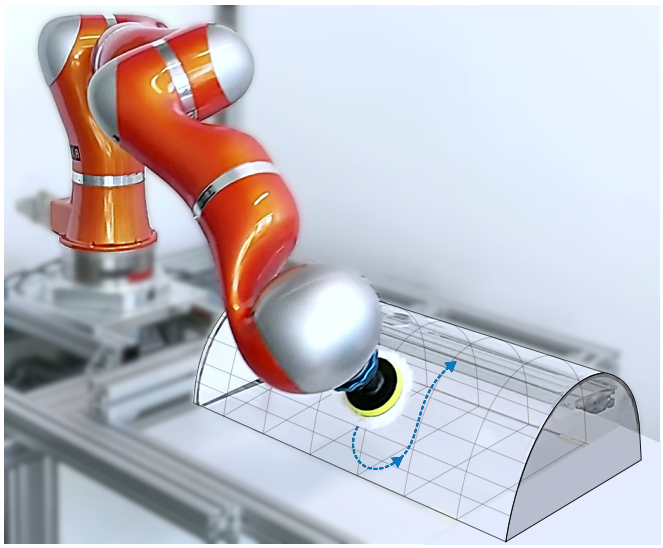

Fig. 1. Polishing a curved surface. The contact force is precisely controlled, while the end-effector is following a trajectory on the structure.

During physical interaction tasks with indirect force control, the environment imposes geometrical constraints on the robotics end-effector. Uncertainties in the model of the environment can potentially generate high contact forces as the desired force is achieved indirectly through the set point of an impedance controller [8], [9]. Thus, to accurately apply desired forces, the environment (surface) geometry and location must be precisely known, which is almost impossible in many real-world applications. Direct force control provides more defined interactions as a detailed environment model is usually unavailable. In practice, explicit force control is often desirable in specific task directions while precise motion control is required in other directions. That leads to hybrid position-force control structures [10]–[12], enabling a direct force control loop in constrained task directions [13], [14]. Commonly, the operational space is partitioned into motion and force subspaces to control the position in the unconstrained task direction [15], [16]. Analysis of standard force control methods and an approach that aims at achieving passivity during interaction by superimposing the motion and force control actions are presented in [17], [18]. Other approaches rely on inverse dynamics control for constrained robots [19]–[21].

In some manipulation tasks, it is beneficial to perform rapid motions while the robot is executing a specific interaction subtask simultaneously. Surface polishing, wiping, and finishing are typical tasks that could be performed in fast motion while regulating the desired contact force. Indeed, modern robotic systems have the capabilities to perform such tasks

© 2023 IEEE. Personal use is permitted, but republication/redistribution requires IEEE permission. See https://www.ieee.org/publications/rights/index.html for more information.

This article has been accepted for publication in IEEE Robotics and Automation Letters. This is the author's version which has not been fully edited and content may change prior to final publication. Citation information: DOI 10.1109/LRA.2023.3270036

that also include physical interaction at high speed. However, this ability to sensitively regulate the contact behavior while moving fast requires to incorporate the respective dynamic effects in the control design. Frequently in force control tasks, the robot is stationary or only moving slowly such that the dynamical terms that depend on velocity and acceleration can be neglected. This is no longer a valid assumption when fast tasks are performed that require accurate contact force control.

This paper focuses on the development of a force-impedance framework to exert well-defined interaction forces while the end-effector is performing fast motions in parallel. The formulation enables to assign constraints in the task space. It can also be interpreted as mixed direct and indirect force control as the proposed scheme features accurate force tracking in constrained directions and compliant behavior in the free motion directions. Moreover, the controller design is carried out in a model-based fashion including these constraints explicitly. The effect of the velocity-dependent couplings is investigated. These terms are usually neglected in the literature. Furthermore, the proposed approach provides a full decoupling of the control actions in the motion and force directions.

The article is organized as follows. Section II introduces the system model to be used throughout this work, and an overview of the standard Cartesian impedance and force control approaches is provided. The proposed hybrid control framework is presented in Section III. Experimental results and validations of the control method compared with the conventional approach are shown and discussed in Section IV. Finally, Section V concludes this article.

II. Fundamentals

The rigid-body dynamics of a manipulator with n degrees of freedom (DOF) can be expressed as

$$\boldsymbol{M}(\boldsymbol{q})\ddot{\boldsymbol{q}} + \boldsymbol{C}(\boldsymbol{q},\dot{\boldsymbol{q}})\dot{\boldsymbol{q}} + \boldsymbol{g}(\boldsymbol{q}) = \boldsymbol{\tau} + \boldsymbol{\tau}^{\mathrm{ext}} \tag{1}$$

with the generalized joint coordinates $\boldsymbol{q} \in \mathbb{R}^n$, the symmetric and positive definite inertia matrix $\boldsymbol{M}(\boldsymbol{q}) \in \mathbb{R}^{n\times n}$, and the Coriolis and centrifugal matrix $\boldsymbol{C}(\boldsymbol{q},\dot{\boldsymbol{q}}) \in \mathbb{R}^{n\times n}$. The term $\boldsymbol{g}(\boldsymbol{q}) \in \mathbb{R}^n$ represents the generalized gravity forces originating from the gravity potential $V_{\mathrm{g}}(\boldsymbol{q})$ through $\boldsymbol{g}(\boldsymbol{q}) = (\partial V_{\mathrm{g}}(\boldsymbol{q})/\partial \boldsymbol{q})^T$. Furthermore, the quantities $\boldsymbol{\tau}, \boldsymbol{\tau}^{\mathrm{ext}} \in \mathbb{R}^n$ describe the generalized joint forces and external forces[1], respectively. The joint forces are assumed to be the control inputs in the following. The applied external wrench $\boldsymbol{F}^{\mathrm{ext}} \in \mathbb{R}^m$ is mapped to external joint torques through a Jacobian matrix $\boldsymbol{J}(\boldsymbol{q}) \in \mathbb{R}^{m\times n}$ according to

$$\boldsymbol{\tau}^{\mathrm{ext}} = -\boldsymbol{J}(\boldsymbol{q})^T\, \boldsymbol{F}^{\mathrm{ext}} \quad , \tag{2}$$

where $m = 6$ if the full Cartesian space is considered. The operational space velocity $\dot{\boldsymbol{y}} \in \mathbb{R}^m$ is described by the mapping $\dot{\boldsymbol{y}} = \boldsymbol{J}(\boldsymbol{q})\,\dot{\boldsymbol{q}}$, which in the general case contains the end-effector translational and rotational velocities. Compliant end-effector behavior can be achieved using the classical impedance control [24]

$$\boldsymbol{\tau}_{\mathrm{imp}} = \boldsymbol{J}(\boldsymbol{q})^T \boldsymbol{F}_{\mathrm{imp}} + \boldsymbol{g}(\boldsymbol{q}) \ , \tag{3}$$

$$\boldsymbol{F}_{\mathrm{imp}} = -\left(\frac{\partial V(\tilde{\boldsymbol{y}})}{\partial \boldsymbol{y}}\right)^T - \boldsymbol{D}_{\boldsymbol{y}}\,\dot{\boldsymbol{y}} \ , \tag{4}$$

where $\boldsymbol{F}_{\mathrm{imp}}$ is the task-space wrench to realize a desired spring-damper behavior, and $V(\tilde{\boldsymbol{x}})$ is the respective positive definite potential function with the virtual spring deflection[2] $\tilde{\boldsymbol{y}} = \boldsymbol{y} - \boldsymbol{y}_{\mathrm{des}}$, where $\boldsymbol{y}$ and $\boldsymbol{y}_{\mathrm{des}} \in \mathbb{R}^m$ are the actual and desired task-space coordinates, respectively. The positive definite damping matrix $\boldsymbol{D}_{\boldsymbol{y}} \in \mathbb{R}^{m\times m}$ is commonly obtained such that critical damping is achieved for varying configurations and different settings of the Cartesian stiffness [25]. In case the robot is equipped with torque sensing capabilities, the joint torque feedback can be used to realize desired dynamics, e. g., to scale down the motor inertia, to provide a link-side torque interface, and vibration-damping. This is a beneficial control strategy when joint-flexibility is considered in the control design to realize the desired joint torques [25]–[27].

In case of environmental constraints, directly controlling the interaction force is beneficial and desirable in many applications. The desired force can be applied simply through

$$\boldsymbol{\tau} = \boldsymbol{\tau}_{\mathrm{imp}} + \boldsymbol{\tau}_{\mathrm{f}} \ , \ \ \boldsymbol{\tau}_{\mathrm{f}} = \boldsymbol{J}(\boldsymbol{q})^T \boldsymbol{F}^{\mathrm{des}} \tag{5}$$

or, as commonly using an explicit force feedback loop as

$$\boldsymbol{\tau}_{\mathrm{f}} = \boldsymbol{J}(\boldsymbol{q})^T \left(\boldsymbol{F}^{\mathrm{des}} - \boldsymbol{K}_{\mathrm{fp}}\tilde{\boldsymbol{F}} - \boldsymbol{K}_{\mathrm{fd}}\dot{\tilde{\boldsymbol{F}}} - \boldsymbol{K}_{\mathrm{fi}}\int_0^t \tilde{\boldsymbol{F}}\,dt\right) \tag{6}$$

where $\tilde{\boldsymbol{F}} = \boldsymbol{F}^{\mathrm{ext}} - \boldsymbol{F}^{\mathrm{des}} \in \mathbb{R}^m$ represents the end-effector wrench error, $\boldsymbol{K}_{\mathrm{fp}}$, $\boldsymbol{K}_{\mathrm{fd}}$, and $\boldsymbol{K}_{\mathrm{fi}}$ are positive-definite proportional, derivative and integral gain matrices, respectively. Here, $\boldsymbol{F}^{\mathrm{ext}}$ is defined in the same direction as $\boldsymbol{F}^{\mathrm{des}}$, forces exerted by the robot on the environment similar to Fig. 2. Furthermore, $\boldsymbol{\tau}_{\mathrm{f}}$ is the generated joint torque to actively achieve the desired force. In principle this provides an enhanced Cartesian force tracking and lower steady-state error due to the propositional-integral actions [3]. The robot dynamic effects in (6) are often neglected since the robot typically moves in a very slow motion (or even stationary) during interaction tasks with specific force characteristics [28]. Different approaches can be used to assign a pure force control in a specific task direction and remove the combined effect of impedance control as in (5)-(6). For example, by splitting the task-space through a selection matrix, [16] or setting the respective directional stiffness to zero and applying a simple superposition [7], [18]. In the following, only force control is considered for the constrained direction.

III. Control Design

Given sufficient knowledge of the environment geometry, the robot should be able to exert the desired interaction forces accurately even while performing highly dynamic motions.

[1]Joint friction is not explicitly considered in the dynamics and it is assumed to be compensated using model-based or observer-based methods [22], [23] .

[2]In impedance control, the desired steady-state position error is often called virtual spring deflection and the set point is frequently called virtual position.

[3]Practically speaking the use of a derivative control action is not common due to the noise in the force signal.

© 2023 IEEE. Personal use is permitted, but republication/redistribution requires IEEE permission. See https://www.ieee.org/publications/rights/index.html for more information.

This article has been accepted for publication in IEEE Robotics and Automation Letters. This is the author's version which has not been fully edited and content may change prior to final publication. Citation information: DOI 10.1109/LRA.2023.3270036

The task space of the end-effector shall have the dimension $m \leq n$. In the case of the full Cartesian space, $m = 6$ including three translations and three rotations. Moreover, kinematic constraints of dimension $c < m$ are imposed on this operational space. As the considered system is kinematically redundant w. r. t. the end-effector, an additional null space of dimension $p = n - m$ exists which can be exploited to simultaneously execute complementary subtasks [4].

The kinematic, holonomic constraints $\boldsymbol{\Phi}(\boldsymbol{q}) \in \mathbb{R}^c$ at the end-effector can be formulated as

$$\boldsymbol{\Phi}(\boldsymbol{q}) = \boldsymbol{0} \ , \tag{7}$$

with $\boldsymbol{\Phi}(\boldsymbol{q})$ being a function with continuous gradient and assumed to be twice differentiable. Without loss of generality a rigid environment is considered. Due to (7) one can represent the constraint as

$$\boldsymbol{J}_{\dot{\boldsymbol{\Phi}}}(\boldsymbol{q})\dot{\boldsymbol{q}} = \boldsymbol{0} \tag{8}$$

with $\boldsymbol{J}_{\dot{\boldsymbol{\Phi}}}(\boldsymbol{q}) = \partial\boldsymbol{\Phi}(\boldsymbol{q})/\partial\boldsymbol{q} \in \mathbb{R}^{c\times n}$. Let $\boldsymbol{x}(\boldsymbol{q}) \in \mathbb{R}^{m-c}$ denote the remaining, unconstrained operational space coordinates with $\boldsymbol{J}_{\dot{\boldsymbol{x}}}(\boldsymbol{q}) = \partial\boldsymbol{x}(\boldsymbol{q})/\partial\boldsymbol{q} \in \mathbb{R}^{(m-c)\times n}$. According to the specification above, the local null space velocities $\boldsymbol{v}(\boldsymbol{q}) \in \mathbb{R}^p$ can be derived using the standard task hierarchy framework [29] through a Jacobian matrix $\boldsymbol{J}_{\boldsymbol{v}}(\boldsymbol{q}) \in \mathbb{R}^{p\times n}$. The stacked Jacobian matrix $\bar{\boldsymbol{J}}(\boldsymbol{q}) \in \mathbb{R}^{n\times n}$ given by

$$\begin{pmatrix} \dot{\boldsymbol{\Phi}} \\ \dot{\boldsymbol{x}} \\ \boldsymbol{v} \end{pmatrix} = \underbrace{\begin{pmatrix} \boldsymbol{J}_{\dot{\boldsymbol{\Phi}}}(\boldsymbol{q}) \\ \boldsymbol{J}_{\dot{\boldsymbol{x}}}(\boldsymbol{q}) \\ \boldsymbol{J}_{\boldsymbol{v}}(\boldsymbol{q}) \end{pmatrix}}_{\bar{\boldsymbol{J}}(\boldsymbol{q})} \dot{\boldsymbol{q}} \tag{9}$$

which is assumed to be invertible in the considered workspace. Due to the constraint $\dot{\boldsymbol{\Phi}} = \boldsymbol{0}$ from (8), solving (9) for $\dot{\boldsymbol{q}}$ yields

$$\dot{\boldsymbol{q}} = \underbrace{\bar{\boldsymbol{J}}(\boldsymbol{q})^{-1} \begin{pmatrix} \boldsymbol{0} & \boldsymbol{0} \\ \boldsymbol{I} & \boldsymbol{0} \\ \boldsymbol{0} & \boldsymbol{I} \end{pmatrix}}_{\boldsymbol{A}(\boldsymbol{q})} \begin{pmatrix} \dot{\boldsymbol{x}} \\ \boldsymbol{v} \end{pmatrix} \ , \tag{10}$$

where $\boldsymbol{A}(\boldsymbol{q}) \in \mathbb{R}^{n\times(n-c)}$ with rank $n - c$. As of now the dependencies on the states are omitted in most of the notations for the sake of readability. The reformulation of (1) yields

$$\bar{\boldsymbol{M}} \begin{pmatrix} \ddot{\boldsymbol{x}} \\ \dot{\boldsymbol{v}} \end{pmatrix} + \bar{\boldsymbol{C}} \begin{pmatrix} \dot{\boldsymbol{x}} \\ \boldsymbol{v} \end{pmatrix} + \bar{\boldsymbol{g}} = \boldsymbol{A}^T\boldsymbol{\tau} - \begin{pmatrix} \boldsymbol{F}^{\text{ext}}_{\dot{\boldsymbol{x}}} \\ \boldsymbol{F}^{\text{ext}}_{\boldsymbol{v}} \end{pmatrix} \tag{11}$$

where $\bar{\boldsymbol{M}} = \boldsymbol{A}^T\boldsymbol{M}\boldsymbol{A} \in \mathbb{R}^{(n-c)\times(n-c)}$ is the inertia matrix for the constrained system, $\bar{\boldsymbol{C}} = \boldsymbol{A}^T\boldsymbol{M}\dot{\boldsymbol{A}} + \boldsymbol{A}^T\boldsymbol{C}\boldsymbol{A}$ denotes the Coriolis and centrifugal matrix, and $\bar{\boldsymbol{g}} = \boldsymbol{A}^T\boldsymbol{g}$ represents the gravitational force. Note that $\boldsymbol{\tau}^{\text{ext}}$ has been rephrased to describe interactions related to the coordinates $\dot{\boldsymbol{\Phi}}$, $\dot{\boldsymbol{x}}$, and $\boldsymbol{v}$ by the respective collocated, generalized forces:

$$\boldsymbol{\tau}^{\text{ext}} = -\bar{\boldsymbol{J}}(\boldsymbol{q})^T \begin{pmatrix} \boldsymbol{F}^{\text{ext}}_{\dot{\boldsymbol{\Phi}}} \\ \boldsymbol{F}^{\text{ext}}_{\dot{\boldsymbol{x}}} \\ \boldsymbol{F}^{\text{ext}}_{\boldsymbol{v}} \end{pmatrix} \tag{12}$$

[4]The null space task will not exist in non-redundant robots when $m = n$.

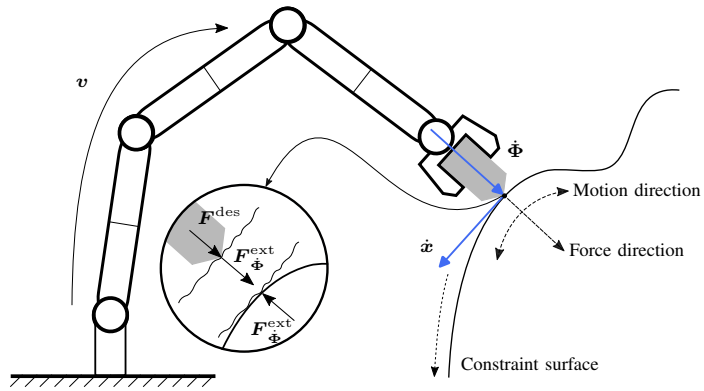

Fig. 2. The concept of the hybrid force-impedance control can be visualized by applying a normal force to an object surface. The motion of the end-effector is constrained by the environment in the direction of the surface normal, while the Cartesian impedance controller operates in the remaining directions. In addition, a null space with different dimensions may exist. The desired force and external interaction forces from the robot and environment perspectives are further highlighted.

In constraint direction no motion exists. However, the dynamic couplings are still of interest, since they influence the contact behavior. Considering (8) on acceleration level,

$$\ddot{\boldsymbol{\Phi}} = \boldsymbol{J}_{\dot{\boldsymbol{\Phi}}}\ddot{\boldsymbol{q}} + \dot{\boldsymbol{J}}_{\dot{\boldsymbol{\Phi}}}\dot{\boldsymbol{q}} = \boldsymbol{0} \ , \tag{13}$$

and substituting (1) and (12), one can compute the predicted *model-based* force $\hat{\boldsymbol{F}}^{\text{ext}}_{\dot{\boldsymbol{\Phi}}}$ in constraint direction as

$$\begin{aligned} \hat{\boldsymbol{F}}^{\text{ext}}_{\dot{\boldsymbol{\Phi}}} &= \boldsymbol{\Lambda}_{\dot{\boldsymbol{\Phi}}}\boldsymbol{J}_{\dot{\boldsymbol{\Phi}}}\boldsymbol{M}^{-1}\left(\boldsymbol{\tau} - \boldsymbol{g} - \boldsymbol{C}\dot{\boldsymbol{q}}\right) + \boldsymbol{\Lambda}_{\dot{\boldsymbol{\Phi}}}\dot{\boldsymbol{J}}_{\dot{\boldsymbol{\Phi}}}\dot{\boldsymbol{q}} \\ &\quad - \boldsymbol{\Lambda}_{\dot{\boldsymbol{\Phi}}}\boldsymbol{J}_{\dot{\boldsymbol{\Phi}}}\boldsymbol{M}^{-1}(\boldsymbol{J}^T_{\dot{\boldsymbol{x}}}\boldsymbol{F}^{\text{ext}}_{\dot{\boldsymbol{x}}} + \boldsymbol{J}^T_{\boldsymbol{v}}\boldsymbol{F}^{\text{ext}}_{\boldsymbol{v}}) \end{aligned} \tag{14}$$

with $\boldsymbol{\Lambda}_{\dot{\boldsymbol{\Phi}}} = (\boldsymbol{J}_{\dot{\boldsymbol{\Phi}}}\boldsymbol{M}^{-1}\boldsymbol{J}^T_{\dot{\boldsymbol{\Phi}}})^{-1}$. The control command is

$$\boldsymbol{\tau} = \boldsymbol{g} + \bar{\boldsymbol{J}}(\boldsymbol{q})^T \begin{pmatrix} \boldsymbol{F}^{\text{ctrl}}_{\dot{\boldsymbol{\Phi}}} \\ \boldsymbol{F}^{\text{ctrl}}_{\dot{\boldsymbol{x}}} \\ \boldsymbol{F}^{\text{ctrl}}_{\boldsymbol{v}} \end{pmatrix} \tag{15}$$

containing gravity compensation, the task control action $\boldsymbol{F}^{\text{ctrl}}_{\dot{\boldsymbol{x}}}$ for the unconstrained end-effector space, $\boldsymbol{F}^{\text{ctrl}}_{\boldsymbol{v}}$ for the null space, and the control action $\boldsymbol{F}^{\text{ctrl}}_{\dot{\boldsymbol{\Phi}}}$ in constraint direction. The control force in the motion directions can be generated as

$$\boldsymbol{F}^{\text{ctrl}}_{\dot{\boldsymbol{x}}} = \boldsymbol{M}_{\boldsymbol{x}}\ddot{\boldsymbol{x}}_{\text{des}} + \boldsymbol{C}_{\boldsymbol{x}}\dot{\boldsymbol{x}}_{\text{des}} - \boldsymbol{K}_{\boldsymbol{x}}\tilde{\boldsymbol{x}} - \boldsymbol{D}_{\boldsymbol{x}}\dot{\tilde{\boldsymbol{x}}} \, . \tag{16}$$

The desired task-space coordinates for the unconstrained space at the end-effector are described by $\boldsymbol{x}_{\text{des}}(t) \in \mathbb{R}^{m-c}$ and the respective error is denoted by $\tilde{\boldsymbol{x}} = \boldsymbol{x} - \boldsymbol{x}_{\text{des}}(t)$. The task specification is characterized by the stiffness and damping matrices $\boldsymbol{K}_{\boldsymbol{x}}, \boldsymbol{D}_{\boldsymbol{x}} \in \mathbb{R}^{(m-c)\times(m-c)}$, while the natural inertia is preserved with (15) [30]. In addition, $\boldsymbol{M}_{\boldsymbol{x}}, \boldsymbol{C}_{\boldsymbol{x}} \in \mathbb{R}^{(m-c)\times(m-c)}$ are task-space inertia and Coriolis and centrifugal matrices in motion direction, respectively. The robot kinematic redundancy can be used to achieve a parallel secondary task in the null space of the end-effector task. For the sake of brevity, $\boldsymbol{F}^{\text{ctrl}}_{\boldsymbol{v}}$ is not specified further here, but w.l.o.g. it can realize arbitrary objectives [5]. Frequent examples are the realization

[5]The null space level requires the dynamically consistent null space projector $\boldsymbol{N} \in \mathbb{R}^{n\times n}$ [31] and the task force $\boldsymbol{F}^{\text{ctrl}}_{\boldsymbol{v}} \in \mathbb{R}^p$. The matrix $\boldsymbol{J}_{\boldsymbol{v}}$ is computed via, $\boldsymbol{J}_{\boldsymbol{v}} = \boldsymbol{J}_2\boldsymbol{N}$ where $\boldsymbol{J}_2$ describes the $p \times n$ Jacobian matrix related to a *subordinate* task, for more details see [29], [32]. Frequent example is $\boldsymbol{F}^{\text{ctrl}}_{\boldsymbol{v}} = -k(q_v - q_{v,\text{d}}) - d\dot{q}_v$ to realize a joint-space impedance with k stiffness, d damping, and $q_{v,\text{d}}$ being the desired equilibrium position of q_v.

© 2023 IEEE. Personal use is permitted, but republication/redistribution requires IEEE permission. See https://www.ieee.org/publications/rights/index.html for more information.

This article has been accepted for publication in IEEE Robotics and Automation Letters. This is the author's version which has not been fully edited and content may change prior to final publication. Citation information: DOI 10.1109/LRA.2023.3270036

of a joint-space impedance or subordinate task-space tracking [29]. The system dynamics can be fully described by using (11), and by inserting the controller (15) that leads to the expression of actuation forces as

$$\boldsymbol{A}^T\boldsymbol{\tau} = \begin{pmatrix} \boldsymbol{F}_{\dot{\boldsymbol{x}}}^{\text{ctrl}} \\ \boldsymbol{F}_{\boldsymbol{v}}^{\text{ctrl}} \end{pmatrix} + \bar{\boldsymbol{g}}\,. \tag{17}$$

For force tracking, (14) must equal the desired force profile $\boldsymbol{F}^{\text{des}}(t) \in \mathbb{R}^c$ which counteracts the interaction forces as

$$\hat{\boldsymbol{F}}_{\dot{\boldsymbol{\Phi}}}^{\text{ext}} - \boldsymbol{F}^{\text{des}}(t) = \boldsymbol{0}\ . \tag{18}$$

Substituting (14) into (18) and inserting (15) delivers

$$\begin{aligned} \boldsymbol{F}_{\dot{\boldsymbol{\Phi}}}^{\text{ctrl}} = &+ \boldsymbol{F}^{\text{des}}(t) \\ &- \boldsymbol{\Lambda}_{\dot{\boldsymbol{\Phi}}}\boldsymbol{J}_{\dot{\boldsymbol{\Phi}}}\boldsymbol{M}^{-1}(\boldsymbol{J}_{\dot{\boldsymbol{x}}}^T\boldsymbol{F}_{\dot{\boldsymbol{x}}}^{\text{ctrl}} + \boldsymbol{J}_{\boldsymbol{v}}^T\boldsymbol{F}_{\boldsymbol{v}}^{\text{ctrl}}) \\ &+ \boldsymbol{\Lambda}_{\dot{\boldsymbol{\Phi}}}\boldsymbol{J}_{\dot{\boldsymbol{\Phi}}}\boldsymbol{M}^{-1}(\boldsymbol{J}_{\dot{\boldsymbol{x}}}^T\boldsymbol{F}_{\dot{\boldsymbol{x}}}^{\text{ext}} + \boldsymbol{J}_{\boldsymbol{v}}^T\boldsymbol{F}_{\boldsymbol{v}}^{\text{ext}}) \\ &+ \boldsymbol{\Lambda}_{\dot{\boldsymbol{\Phi}}}(\boldsymbol{J}_{\dot{\boldsymbol{\Phi}}}\boldsymbol{M}^{-1}\boldsymbol{C} - \dot{\boldsymbol{J}}_{\dot{\boldsymbol{\Phi}}})\dot{\boldsymbol{q}}\ . \end{aligned} \tag{19}$$

One of the main differences to state-of-the-art approaches for force tracking is the last component in (19), which is usually neglected in the control design and becomes particularly relevant for highly dynamic motions as shown in the experiments in Sec. IV. Note that in frictionless contacts and the absence of external forces in $\dot{\boldsymbol{x}}$- and $\boldsymbol{v}$-direction the terms $\boldsymbol{F}_{\dot{\boldsymbol{x}}}^{\text{ext}}$ and $\boldsymbol{F}_{\boldsymbol{v}}^{\text{ext}}$ vanish in (19), which significantly simplifies the control feedback. Notably, the third term of the control law compensates for the dynamic coupling w. r. t. the external forces present in the free directions of motion and the null space. Moreover, an additional proportional-integral term can support to reduce steady-state errors in the contact force. Therefore, the optional term

$$\boldsymbol{F}_{\text{PI}} = -\boldsymbol{k}_{\text{P}}(\boldsymbol{F}_{\dot{\boldsymbol{\Phi}}}^{\text{ext}} - \boldsymbol{F}^{\text{des}}(t)) - \boldsymbol{k}_{\text{I}}\int(\boldsymbol{F}_{\dot{\boldsymbol{\Phi}}}^{\text{ext}} - \boldsymbol{F}^{\text{des}}(t))\,dt \tag{20}$$

with control gains $\boldsymbol{k}_{\text{P}}, \boldsymbol{k}_{\text{I}}$ can be added to the previous control law (19). Feedback of $\boldsymbol{F}_{\dot{\boldsymbol{\Phi}}}^{\text{ext}}$ can be easily implemented using a modern design of end-effector external wrench observer [33]. Furthermore, the obtained control law (19) is gain-free in contact-force direction, which is an advantage w. r. t. the tuning effort. Figure 2 illustrates a conceptual scenario, the kinematic constraint is active in end-effector normal direction, and the unconstrained task is given by the end-effector motion (e. g., to track a specific profile). The local null space velocity $\boldsymbol{v}$ represents the one-dimensional null space behavior. If full dynamical decoupling is not provided by control, as commonly done by the conventional approach, see (6), force errors are to be expected during highly dynamic and fast motions. Consequently, contact force deviations could potentially generate higher joint torques and velocities reaching the saturation limits, especially when impacts occur with the constraint surface. In fact, this makes the feedback control gains valid only locally and tuned at specific task speeds. In contrast, the proposed control law in (15) avoids such problems as a full dynamical decoupling is achieved.

Usually, the force controller is not required at all times. It is only used when contact with the environment is already established. To have continuous and smooth force-impedance transitions, an intermediate desired value has been introduced [34]. This rapid transition between different control actions can lead to discontinuous behavior in the commanded joint torques. To avoid this discontinuity, an intermediate desired value can be used such that the control input does not instantly change. This is done using activation variables changing continuously from 0 to 1 and specifying which controller is selected in a smooth manner. With sufficient geometrical knowledge about the environment, one can increase the gains of the impedance controller (set higher stiffness values) in the free motion directions as the interactions in those directions are less likely. In this way, better trajectory position tracking performance can be achieved at the end-effector level.

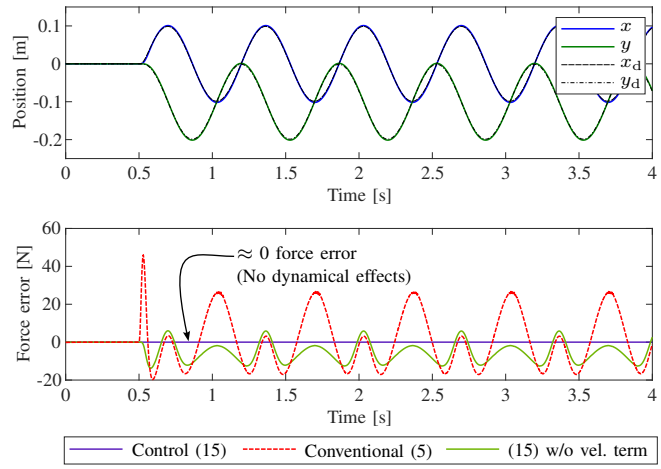

Fig. 3. Simulation #1: applying a constant desired end-effector force in z-direction while performing a circular motion in x/y-directions.

The proposed approach shares similar aims to the widely known category of hybrid force-motion control since the motion is controlled in the free task direction, and the force is controlled in the constrained directions of the task. Here, instead of using a stiff position controller [15], a Cartesian impedance controller is used such that the stiffness in the free directions is also parameterized. Actually, it can also be interpreted as mixed direct and indirect force control as it is categorized in [8], [9]. Moreover, the selection of the force and motion subspaces could be done in a straightforward fashion using the concept of selection matrix [15], [16] or combine the force tracking with the impedance control [18] such that the separation is no more needed.

IV. Simulations and Experiments

The proposed hybrid controller is validated in simulations and experiments on a DLR-KUKA LWR IV+ torque-controlled robot. The controller runs at a rate of 1 kHz, while the low joint-level torque controller is executed at 3 kHz. A Cartesian impedance controller is used to close the initial contact between the robotic end-effector and the constraint surface. In the proposed framework, both force- and impedance control are assigned to the same priority level as mentioned in Section III. Therefore, it may be widely known under the category of hybrid force-motion control. The desired task-space translational and rotational stiffness and damping values used in simulation and experiments are summarized

© 2023 IEEE. Personal use is permitted, but republication/redistribution requires IEEE permission. See https://www.ieee.org/publications/rights/index.html for more information.

This article has been accepted for publication in IEEE Robotics and Automation Letters. This is the author's version which has not been fully edited and content may change prior to final publication. Citation information: DOI 10.1109/LRA.2023.3270036

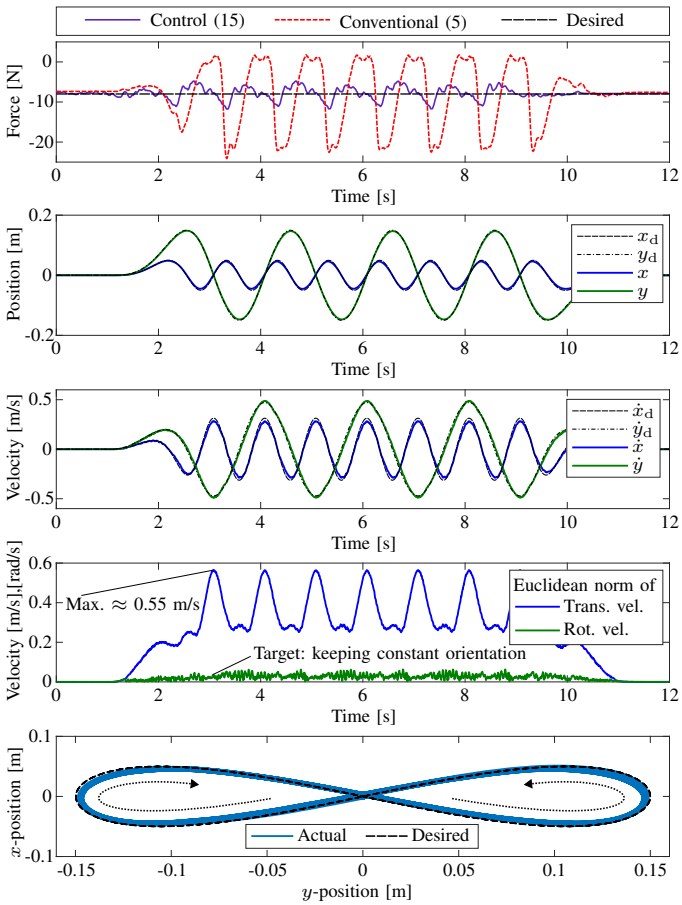

Fig. 4. Experiment #1: the robot end-effector is kept normal to a flat surface while executing a dynamically demanding trajectory (eight-shape motion). The applied force in constraint direction is shown in the top chart. The second and third diagrams illustrate the desired and the actual trajectories. The Euclidean norm of translational and rotational velocities and a top view of the Cartesian trajectories of the end-effector position are shown in the bottom charts.

TABLE I
CONTROL GAINS FOR SIMULATION AND EXPERIMENTS

Parameter	Simulation	Experiments
Transl. Cart. impedance	5000 [N/m]	1500 [N/m]
Rot. Cart. impedance	500 [Nm/rad]	300 [Nm/rad]
Damping ratio	0.7	0.7

in Table I.[6] The interaction force could be computed from different sources, e. g., via joint-space external force observers [35] or explicit force-torque sensors. Alternatively, an extended momentum-based observer [33] could be deployed to obtain the contact force measurement in task space directly.

In the following Simulation #1, a task is assigned in which the manipulator performs fast motions in the x-y-plane (free directions) and exerts a desired contact force on the surface (normal/constrained direction). MATLAB/Simulink is used for the robot simulation. The desired and actual trajectories are shown in Fig. 3 (top diagram) along with the corresponding force errors (bottom diagram). Theoretically speaking, the proposed approach shows zero error as full dynamic compensation is achieved. Additionally, the effect of velocity-dependent terms in the overall hybrid-controller is highlighted by setting $\dot{\boldsymbol{q}}$ to zero in the last component of the control feedback

[6]The Cartesian damping matrix $\boldsymbol{D}_x$ is designed to achieve critical damping in the modal space of the free task directions for varying robot configurations.

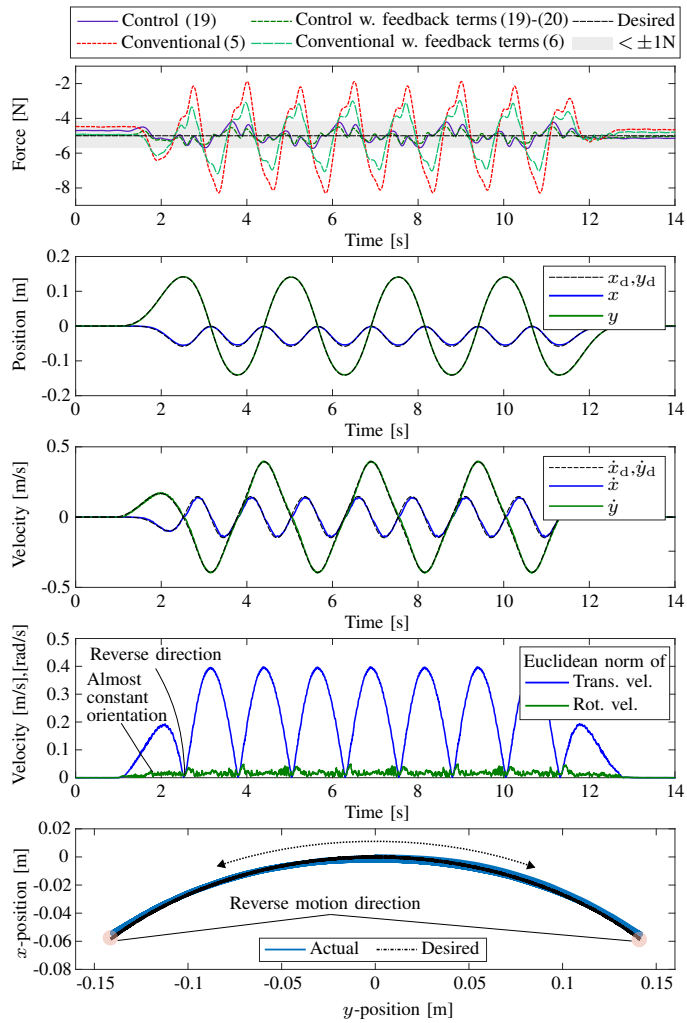

Fig. 5. Experiment #2 moving on a flat surface with an arc-like shape to investigate the effect of the choice of the control gains. The force tracking performance is included in case of setting the control gains to zero in (6) and (20), shown in the top diagram. The position and velocity of the desired and actual trajectories are plotted in the second and third diagrams, respectively. The Euclidean norm of the end-effector velocity is shown in the fourth diagram. The bottom diagram depicts the two-dimensional view of the desired (black) and actual (blue) trajectories.

in (19). Experiment #1 demonstrates the force tracking performance by controlling the normal contact force along a flat surface and executing a highly dynamic desired motion trajectory simultaneously. The actual and desired trajectories are depicted in Fig. 4 with maximum end-effector translational velocity norm attaining values of $\approx$ 0.55 m/s. Therein, the force tracking performance (top diagram), the position and velocity of the applied trajectory, and the Euclidean norms of the Cartesian velocity are plotted, respectively. In this case the robot reached a considerable translational velocity as shown in Fig. 4. Notably, the proposed method features a superior force tracking performance compared to the conventional technique. The remaining force error in the proposed method is due to the fact that the force control law has been obtained based on some ideal assumptions such as interacting with rigid environments, no flexibility in the robotic system, and perfect dynamic model. These un-modeled dynamics can be treated as a disturbance, and an additional integrator e. g. (20) might be sufficient to deal with these unpredictable errors and

© 2023 IEEE. Personal use is permitted, but republication/redistribution requires IEEE permission. See https://www.ieee.org/publications/rights/index.html for more information.

This article has been accepted for publication in IEEE Robotics and Automation Letters. This is the author's version which has not been fully edited and content may change prior to final publication. Citation information: DOI 10.1109/LRA.2023.3270036

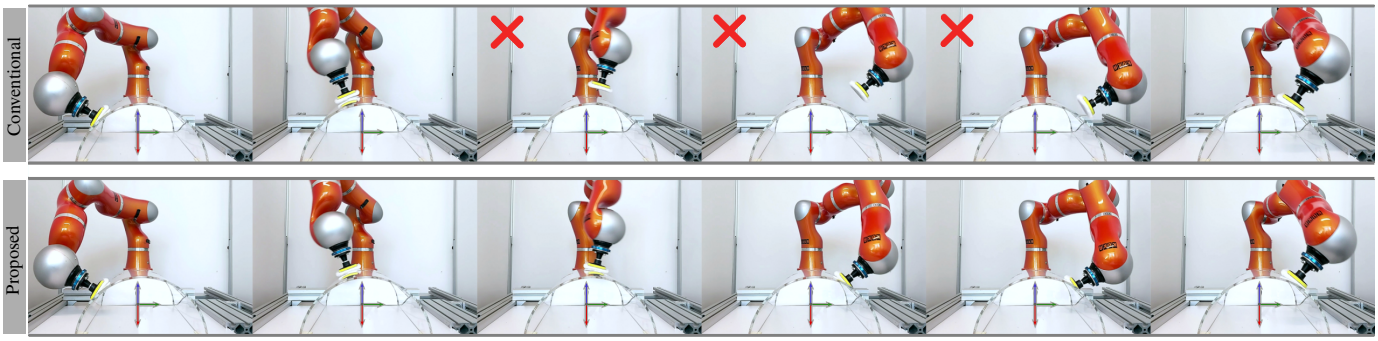

Fig. 6. Experiment #3a: Fast surface polishing scenario is illustrated by controlling the contact on curved surface. The motion sequence for the conventional method (top row) and the proposed approach (bottom row) are shown. The contact is lost during high-velocity phases (marked with red ×) due to velocity-dependent dynamical coupling effects within the conventional approach; see the video attachment.

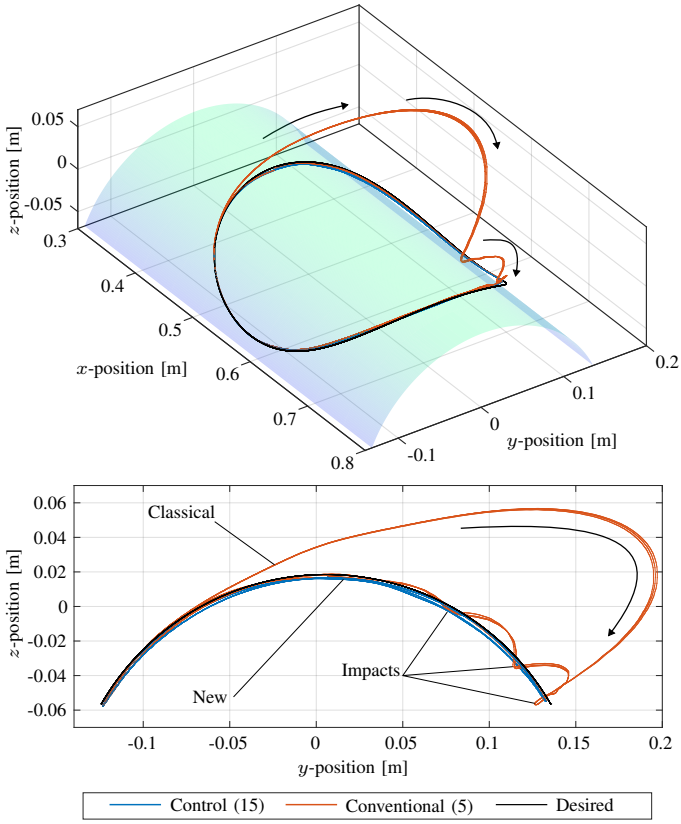

Fig. 7. Experiment #3b (fast trajectory on curved surface): Highly dynamic desired trajectory applied on the cylindrical object. In the classical method, the contact with the target object is lost, resulting in large errors.

increase the robustness against steady-state force deviations. Note that the friction forces (e. g. surface friction) are already included through the feedback of the task-space external forces $\boldsymbol{F}_{\dot{\boldsymbol{x}}}^{\text{ext}}$ in (19), which is obtained through observer-based methods [35]. In the experiments, a wool-polishing tool is used as end-effector; see the attached video.

Experiment #2 is performed to validate the effect of including gains within the force control loop as in (6). It is worth mentioning that the inclusion of force feedback gains reduces the capability of moving at high velocity due to the presence of instabilities caused by the additional control action (PI/PID) related to contact force deviations. The end-effector, in this case, follows a simple arc-like trajectory designed to provide fair conditions for a comparison with the state-of-the-art approach, see Fig. 5. The parameters are tuned to achieve the best possible performance of the classical approach in terms of contact force error. Expectedly, the force control gains reduced the steady-state error and the dynamic force oscillations but at the cost of performing the motion with lower velocity for not losing the contact. Nevertheless, the proposed approach shows lower force error than the conventional method. It can be seen that the effect of the force feedback terms is minor for the proposed method and can be ignored while not reducing the performance. In fact, that increases the robustness and simplifies the implementation of the controller.

In Experiment #3, the capability to perform highly dynamic motions on the surface of a curved object (acrylic cylindrical part) is illustrated. The task reassembles/represents a high-speed surface polishing scenario where the contact force over a curved surface is maintained. Figure 6 shows a photo series at different points of time for the performed task using the classical method (top row) and the proposed approach (bottom row). It can be clearly seen that using the classical method caused a high deviation in the direction of the surface normal due to the loss of contact with the target object. The end-effector trajectories are depicted in Fig. 7. Notably the contact loss occurs multiple times during the applied trajectory and results in impacts with the surface, see Fig. 8. The proposed approach shows superior performance in terms of force tracking while following a dynamically demanding trajectory on a curved surface. The non-contact phases are highlighted (shaded areas) in Fig. 8 which can be related to the Euclidean norm of the joint velocities $\|\dot{\boldsymbol{q}}\|$ (diagram 6). Interestingly, the high velocities lead to the contact-loss (lift-off) phases even at similar task-space velocity, see diagram 5. The end-effector force tracking is depicted in diagram 1 of Fig. 8. The position and velocity of the applied trajectory expressed in the robot base frame are shown in diagrams 2 and 3, respectively. The end-effector translational velocity norm is shown in diagram 4, the rotational velocity norm in diagram 5, the joint space velocity norm in diagram 6, and the tool-surface positional deviation (the distance along the surface normal) in the bottom diagram. Geometrically speaking, the total desired translational velocity is approximately constant over the curved surface. However, the rotational velocity changes continuously along the applied trajectory by the effect of change of curvature w. r. t. the end-effector motion. That means

© 2023 IEEE. Personal use is permitted, but republication/redistribution requires IEEE permission. See https://www.ieee.org/publications/rights/index.html for more information.

This article has been accepted for publication in IEEE Robotics and Automation Letters. This is the author's version which has not been fully edited and content may change prior to final publication. Citation information: DOI 10.1109/LRA.2023.3270036

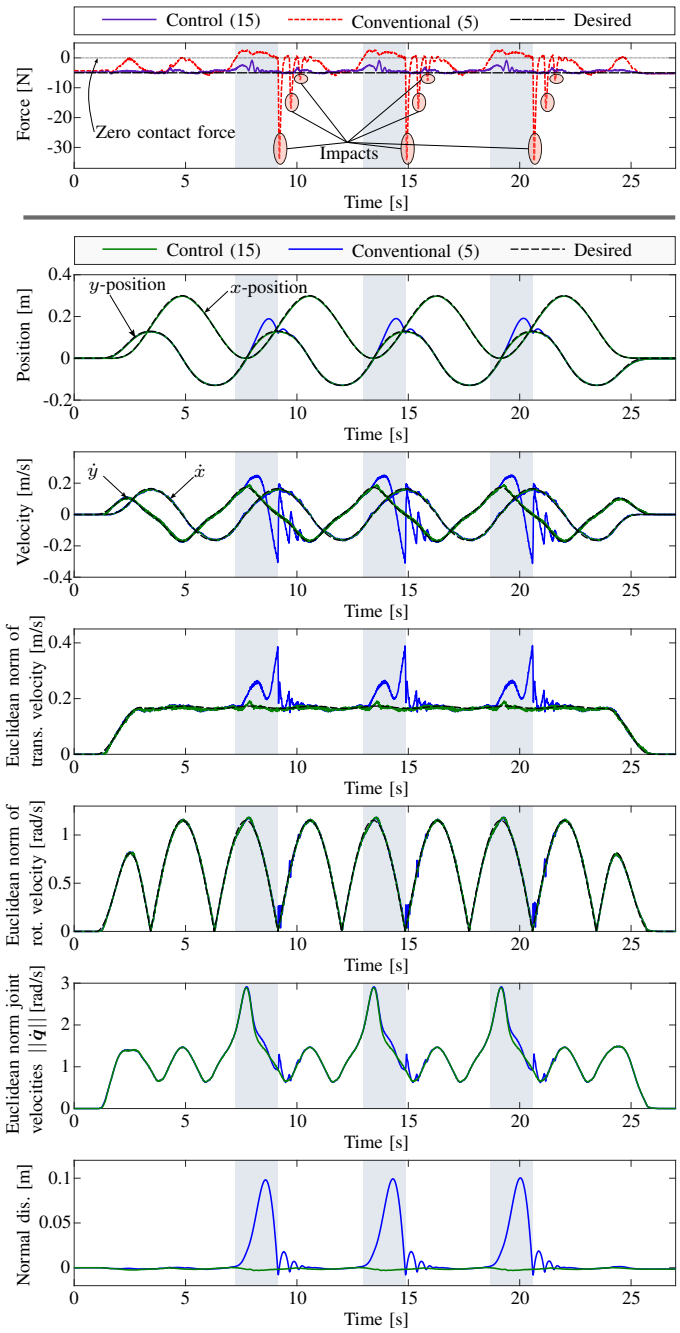

Fig. 8. Experiment #3c (fast contact on a curved surface): The trajectory is commanded to reach the maximum possible velocity before actuator saturation. The highlighted (shaded) areas represent contact loss due to high dynamical couplings during those phases.

the considered trajectory reaches constant/zero curvature when the end-effector motion is purely in x-direction (completely aligned with x-direction) and high values when the motion occurs in perpendicular direction. The maximum joint-space velocity of $\approx$ 2.9 rad/s, which is very close to the saturation limit, is achieved during the peaks of the task-space rotational velocity. During the highly dynamic phases, the proposed approach shows significantly better control performance in contact force direction. It is worth mentioning that in this experimental setting, the conventional approach is not able to maintain the contact at approximately 0.8 rad/s of joint velocity norm, which corresponds to peak end-effector translational and

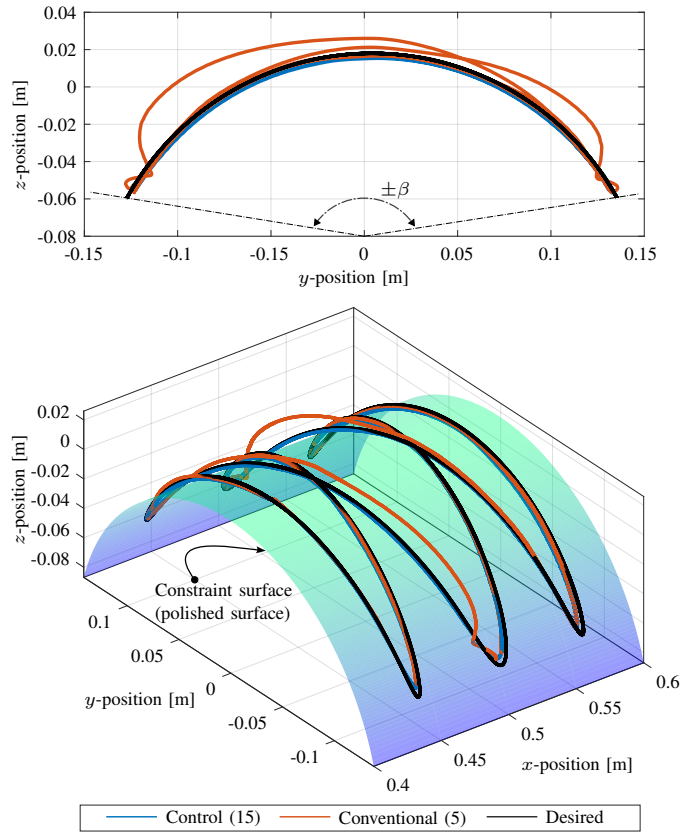

Fig. 9. Experiment #4a: (variable desired force): A complex trajectory is applied to the object under surface polishing operation. The desired normal force (contact pressure) is varied over time simultaneously. The top and bottom diagrams show front and three-dimensional views of the desired and actual trajectories, respectively.

rotational velocities of 0.05 m/s and 0.8 rad/s, respectively.

The evaluation of the force tracking performance in Experiment #4 is conducted by commanding the desired force trajectory and following a specific path on a curved surface simultaneously. Figure 9 shows the three-dimensional view of the desired and actual positions for the conventional and proposed method, respectively. The trajectory is expressed using a cylindrical angle β and the longitudinal axis x such that visual separation between the motion and the force subspaces is obtained. The time-varying force trajectory and the end-effector force tracking error are illustrated in diagrams 1 and 2 of Fig. 10. The applied trajectory position, and task-space translational and rotational velocity norms expressed in the robot base frame are shown in diagrams 3 and 4, respectively.

The goal of the proposed control structure is to decouple the force and motion subspaces. The control scheme allows simultaneous tracking of both contact force and end-effector-compliant motion independently and at the same priority level. Therefore, the control design was carried out through a model-based approach to be able to fully compensate for the velocity-dependent terms as well as take into account the other control actions and external forces. The importance of this method is raised during the execution of fast motion trajectories and simultaneous control of the contact force. The proposed control structure has a significant effect during highly dynamic motion execution over curved surfaces compared to

© 2023 IEEE. Personal use is permitted, but republication/redistribution requires IEEE permission. See https://www.ieee.org/publications/rights/index.html for more information.

This article has been accepted for publication in IEEE Robotics and Automation Letters. This is the author's version which has not been fully edited and content may change prior to final publication. Citation information: DOI 10.1109/LRA.2023.3270036

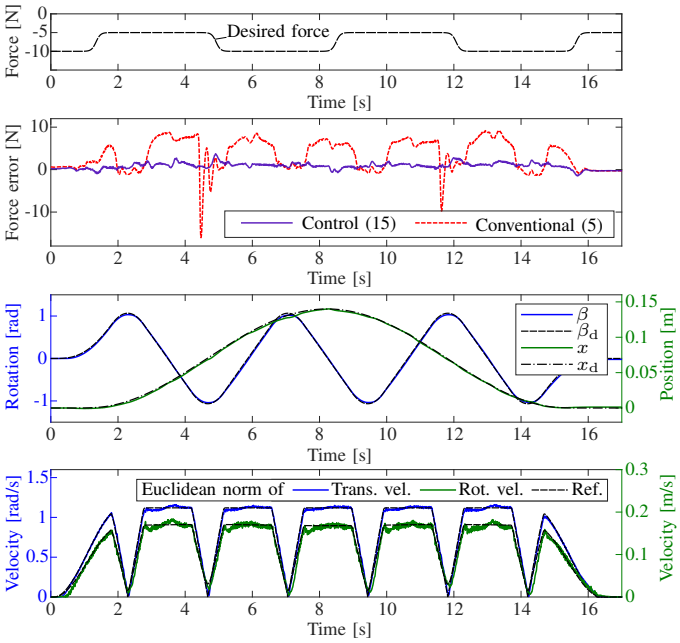

Fig. 10. Experiment #4b: (time-varying force profile): The desired contact force is varied between 5 and 10 N. The force tracking error is shown in the top diagram, followed by the desired and actual (measured) forces. The trajectory expressed in polar/cylindrical coordinates is depicted in diagram 3, and the task velocity norms are shown in the bottom diagram.

the conventional approach. The experimental results confirm that considering the velocity dependency in the force control law seems to be necessary in fast force-controlled tasks.

V. Conclusion

A unified hybrid force-impedance framework for highly dynamic end-effector motions was presented. In addition to the complaint behavior in the free motion directions, the approach provides precise force tracking in constrained contact direction. The control formulation allows the straightforward integration of the end-effector geometrical constraints, yielding full dynamical decoupling between the force- and motion-subspaces. Simulations and experiments including flat and curved surfaces showed the high performance of the proposed method and confirmed the theoretical claims in highly demanding dynamic motions.

References

[1] N. Hogan, "Impedance Control: An Approach to Manipulation: Part I, Part II, Part III," *Journal of Dynamic Systems, Measurement, and Control*, vol. 107, pp. 1–24, March 1985.

[2] W. S. Newman, "Stability and performance limits of interaction controllers," 1992.

[3] D. Lee and K. Huang, "Passive-set-position-modulation framework for interactive robotic systems," *IEEE TRO*, vol. 26, no. 2, 2010.

[4] E. Lutscher et al., "Hierarchical force and positioning task specification for indirect force controlled robots," *IEEE TRO*, 2017.

[5] F. Ficuciello, L. Villani, and B. Siciliano, "Variable impedance control of redundant manipulators for intuitive human–robot physical interaction," *IEEE Transactions on Robotics*, vol. 31, no. 4, pp. 850–863, 2015.

[6] L. Chen, L. F. Figueredo, and M. R. Dogar, "Planning for muscular and peripersonal-space comfort during human-robot forceful collaboration," in *2018 Humanoids*. IEEE, 2018, pp. 1–8.

[8] B. Siciliano and L. Villani, *Robot force control*. Springer Science & Business Media, 1999.

[7] M. Dyck, A. Sachtler, J. Klodmann, and A. Albu-Schäffer, "Impedance control on arbitrary surfaces for ultrasound scanning using discrete differential geometry," *IEEE RA-L*, vol. 7, no. 3, pp. 7738–7746, 2022.

[9] L. Villani and J. De Schutter, "Force control," in *Springer handbook of robotics*. Springer, 2016, pp. 195–220.

[10] T. Yoshikawa, "Dynamic hybrid position/force control of robot manipulators–description of hand constraints and calculation of joint driving force," *IEEE Journal on Robotics and Automation*, 1987.

[11] N. H. McClamroch and D. Wang, "Feedback stabilization and tracking of constrained robots," *IEEE Transactions on Automatic Control*, vol. 33, no. 5, pp. 419–426, 1988.

[12] J. K. Mills and A. A. Goldenberg, "Force and position control of manipulators during constrained motion tasks," *IEEE Transactions on Robotics and Automation*, vol. 5, no. 1, pp. 30–46, 1989.

[13] V. Ortenzi, M. Adjigble, J. A. Kuo, R. Stolkin, and M. Mistry, "An experimental study of robot control during environmental contacts based on projected operational space dynamics," in *2014 Humanoids*. IEEE.

[14] R. Volpe and P. Khosla, "A theoretical and experimental investigation of explicit force control strategies for manipulators," *IEEE Transactions on Automatic Control*, vol. 38, no. 11, pp. 1634–1650, 1993.

[15] M. H. Raibert and J. J. Craig, "Hybrid Position/Force Control of Manipulators," *Journal of Dynamic Systems, Measurement, and Control*, vol. 103, no. 2, pp. 126–133, 06 1981.

[16] O. Khatib, "A Unified Approach for Motion and Force Control of Robot Manipulators: The Operational Space Formulation," *IEEE Journal of Robotics and Automation*, vol. RA-3, no. 1, pp. 43–53, February 1987.

[17] G. Zeng and A. Hemami, "An overview of robot force control," *Robotica*, vol. 15, no. 5, pp. 473–482, 1997.

[18] C. Schindlbeck and S. Haddadin, "Unified passivity-based cartesian force/impedance control for rigid and flexible joint robots via task-energy tanks," in *2015 ICRA*. IEEE, 2015, pp. 440–447.

[19] F. Aghili, "A unified approach for inverse and direct dynamics of constrained multibody systems based on linear projection operator: applications to control and simulation," *IEEE TRO*, vol. 21, no. 5, 2005.

[20] N. Mansard, O. Khatib, and A. Kheddar, "A Unified Approach to Integrate Unilateral Constraints in the Stack of Tasks," *IEEE Transactions on Robotics*, vol. 25, no. 3, pp. 670–685, June 2009.

[21] M. Mistry, J. Buchli, and S. Schaal, "Inverse dynamics control of floating base systems using orthogonal decomposition," in *2010 ICRA*. IEEE.

[22] M. Iskandar and S. Wolf, "Dynamic friction model with thermal and load dependency: modeling, compensation, and external force estimation," in *2019 ICRA*. IEEE, May 2019, pp. 7367–7373.

[23] S. Wolf and M. Iskandar, "Extending a dynamic friction model with nonlinear viscous and thermal dependency for a motor and harmonic drive gear," in *2018 ICRA*. IEEE, May 2018, pp. 783–790.

[24] F. Caccavale, C. Natale, B. Siciliano, and L. Villani, "Six-dof impedance control based on angle/axis representations," *IEEE Transactions on Robotics and Automation*, vol. 15, no. 2, pp. 289–300, 1999.

[25] A. Albu-Schäffer, C. Ott, and G. Hirzinger, "A Passivity Based Cartesian Impedance Controller for Flexible Joint Robots - Part II: Full State Feedback, Impedance Design and Experiments," in *Proc. of the 2004 ICRA*, April 2004, pp. 2666–2672.

[26] ——, "A Unified Passivity-based Control Framework for Position, Torque and Impedance Control of Flexible Joint Robots," *International Journal of Robotics Research*, vol. 27, no. 1, pp. 23–39, January 2007.

[27] M. Iskandar et al., "Joint-level control of the dlr lightweight robot sara," in *Proc. of the 2020 IEEE/RSJ IROS*. IEEE, 2020.

[28] D. Leidner, A. Dietrich, M. Beetz, and A. Albu-Schäffer, "Knowledge-enabled parameterization of whole-body control strategies for compliant service robots," *Autonomous Robots*, vol. 40, no. 3, pp. 519–536, 2016.

[29] A. Dietrich and C. Ott, "Hierarchical Impedance-Based Tracking Control of Kinematically Redundant Robots," *IEEE TRO*, February 2020.

[30] A. Dietrich et al., "Practical consequences of inertia shaping for interaction and tracking in robot control," *Control Engineering Practice*, vol. 114, p. 104875, 2021.

[31] A. Dietrich, C. Ott, and A. Albu-Schäffer, "An overview of null space projections for redundant, torque-controlled robots," *IJRR*, vol. 34, no. 11, pp. 1385–1400, Sept. 2015.

[32] M. Iskandar et al., "Employing whole-body control in assistive robotics," in *IEEE IROS*, November 2019, pp. 5643–5650.

[33] M. Iskandar, O. Eiberger, A. Albu-Schäffer, A. De Luca, and A. Dietrich, "Collision detection, identification, and localization on the dlr sara robot with sensing redundancy," in *2021 ICRA*. IEEE, 2021, pp. 3111–3117.

[34] J. Lee, N. Mansard, and J. Park, "Intermediate Desired Value Approach for Task Transition of Robots in Kinematic Control," *IEEE TRO*.

[35] A. De Luca, A. Albu-Schäffer, S. Haddadin, and G. Hirzinger, "Collision Detection and Safe Reaction with the DLR-III Lightweight Manipulator Arm," in *Proc. of the 2006 IROS*, October 2006, pp. 1623–1630.

© 2023 IEEE. Personal use is permitted, but republication/redistribution requires IEEE permission. See https://www.ieee.org/publications/rights/index.html for more information.